CHEMISTRY OF MATERIALS

UNIVERSITY OF TECHNOLOGY SYDNEY

Subscriber access provided by UNIVERSITY OF TECHNOLOGY SYDNEY

Article

Molecular Layer Etching of Metalcone Films Using Lithium Organic Salts and Trimethylaluminum

Matthias J. Young, Devika Choudhury, Steven Letourneau, Anil Mane, Angel Yanguas-Gil, and Jeffrey W. Elam

Chem. Mater., **Just Accepted Manuscript** • DOI: 10.1021/acs.chemmater.9b03627 • Publication Date (Web): 15 Jan 2020

Downloaded from pubs.acs.org on January 22, 2020

Just Accepted

"Just Accepted" manuscripts have been peer-reviewed and accepted for publication. They are posted online prior to technical editing, formatting for publication and author proofing. The American Chemical Society provides "Just Accepted" as a service to the research community to expedite the dissemination of scientific material as soon as possible after acceptance. "Just Accepted" manuscripts appear in full in PDF format accompanied by an HTML abstract. "Just Accepted" manuscripts have been fully peer reviewed, but should not be considered the official version of record. They are citable by the Digital Object Identifier (DOI®). "Just Accepted" is an optional service offered to authors. Therefore, the "Just Accepted" Web site may not include all articles that will be published in the journal. After a manuscript is technically edited and formatted, it will be removed from the "Just Accepted" Web site and published as an ASAP article. Note that technical editing may introduce minor changes to the manuscript text and/or graphics which could affect content, and all legal disclaimers and ethical guidelines that apply to the journal pertain. ACS cannot be held responsible for errors or consequences arising from the use of information contained in these "Just Accepted" manuscripts.

is published by the American Chemical Society. 1155 Sixteenth Street N.W., Washington, DC 20036

Published by American Chemical Society. Copyright © American Chemical Society. However, no copyright claim is made to original U.S. Government works, or works produced by employees of any Commonwealth realm Crown government in the course of their duties.

1
2
3
4
5
6
7
8
9
10
11
12
13
14
15
16
17
18
19
20
21
22
23
24
25
26
27
28
29
30
31
32
33
34
35
36
37
38
39
40
41
42
43
44
45
46
47
48
49
50
51
52
53
54
55
56
57
58
59
60

Molecular Layer Etching of Metalcone Films Using Lithium Organic Salts and Trimethylaluminum

Matthias J. Young,[1,2,3] Devika Choudhury,[1] Steven Letourneau,[1] Anil Mane,[1] Angel Yanguas-Gil, Jeffrey W. Elam[1*]

[1] Applied Materials Division, Argonne National Laboratory, Lemont, Illinois, 60439

[2] Department of Biomedical, Biological, and Chemical Engineering, University of Missouri, Columbia, MO, 65211

[3] Department of Chemistry, University of Missouri, Columbia, MO, 65211

*Email: jelam@anl.gov

I. Abstract

Advances in semiconductor device manufacturing are limited by our ability to precisely add and remove thin layers of material in multistep fabrication processes. Recent reports on atomic layer etching (ALE) have provided the means for precise removal of inorganic thin films deposited by atomic layer deposition (ALD), opening new avenues for nanoscale device design. Here we report on a new technique for the precise removal of metal organic thin films deposited by molecular layer deposition (MLD), which we term molecular layer etching (MLE). This etching process employs sequential exposures of lithium organic salt (LOS) and trimethylaluminum (TMA) precursors to produce self-limiting etching behavior. We employ quartz crystal microbalance (QCM) experiments to demonstrate (a) etching of alucone films preloaded with LOS upon TMA exposures and (b) layer-by-layer etching of alucone films using alternating exposures of LOS and TMA. We also identify selectivity of these etching mechanisms. We probe the mechanism for the layer-by-layer etching of alucone using quartz crystal microbalance and Fourier transform infrared spectroscopy, and identify that the etching proceeds via heterolytic cleaving of Al-O bonds in alucone upon LOS exposure, followed by methylation to produce volatile species upon TMA exposure. The etching process results in the removal of 0.4 nm/cycle of alucone at 160°C and up to 3.6 nm/cycle of alucone at 266°C in ex situ etching experiments on silicon wafers. This halogen-free etching process enables etching of MLD films and provides new fabrication pathways for the control of material geometries at the nanoscale.

II. Introduction

Starting in the mid-20th century through the early 21st century, the semiconductor community has been able to maintain Moore's law scaling[1] by herculean effort, driving the number of transistors per unit area ever-higher with reports in 2019 of ~10^9 devices/cm^2 in line with nominal 7 nm transistor architectures.[2] In order to keep up with Moore's law, semiconductor device geometries have become increasingly complex. Notably, metal oxide semiconductor field effect transistors (MOSFETs) have shifted from their original 2D architectures to 3D fin field effect transistors (FinFET)[3] and gate-all-around (GAA) architectures[4] to pack more transistors per unit area. Fabricating these nanoscale architectures has required a range of advances in semiconductor manufacturing processes. One area of innovation enabling these devices has been in the ability to provide precision thinning for formation of fins for FinFETs. During initial development of

FinFETs, the formation of fins was accomplished using an anisotropic halogen etch (e.g. HF, Cl_2) coupled with Ar^+ ion bombardment to form fins in silicon wafers. This initial formation step was followed by an isotropic dry-etch under reactive halogen exposure and heat treatment at high temperature (up to 1000°C) to form the fin.[3]

More recently, the development of thermal atomic layer etching (ALE) using gas phase chemical precursors has enabled isotropic etching at constant temperature with improved etching resolution. ALE is an etching analog of atomic layer deposition (ALD).[5] Both ALD and ALE rely on sequential, gas-phase surface reactions. However, while ALD is used to *deposit* material with atomic scale precision, ALE is used to *remove* material with atomic scale precision. In typical ALE schemes, the material surface is converted to a metal fluoride through HF exposure, then an organometallic precursor is dosed which undergoes ligand exchange with this surface fluoride. This ligand exchange generates volatile species comprised of metal centers bound to both organic ligands and fluorine.[6] ALE was first reported for etching Al_2O_3 using hydrogen fluoride (HF) and tin(II) acetylacetonate ($Sn(acac)_2$).[7] Initial studies[6–9] on the etching of Al_2O_3 have expanded to include thermal etching of a number of relevant materials for semiconductor manufacturing including Si,[10] SiO_2,[11] HfO_2,[12] ZnO,[13] TiO_2,[14] TiN,[15] W and WO_3,[16] among others.[17] Further work has also identified pathways for selective ALE.[18] However, there are a number of opportunity areas to improve upon these established ALE chemistries. For example, current ALE chemistries are limited to etching of inorganic materials, use harsh halogen precursors, and produce only modest etch rates—on the order of 1 Å/cycle or lower.

Here, we report on the discovery of a new etching process which we term molecular layer etching, or MLE. Just as ALE is the etching analog of ALD, the MLE process we report is the etching analog of molecular layer deposition (MLD). MLD employs organic precursors to deposit organic or metal organic thin films.[19–21] While initial reports on MLD focused on polymeric films, later efforts combined organic and organometallic precursors to form hybrid metal organic thin films by MLD. The first reported hybrid metal organic MLD chemistry employed trimethylaluminum (TMA) and ethylene glycol (EG) to deposit a thin film material termed "alucone"[22] followed shortly thereafter by studies employing TMA with hydroquinone and phloroglucinol.[23] Further studies reported the growth of a range of metal organic thin films, or "metalcones," by combining organometallic precursors and bifunctional organic molecules.[22,24,25] These metalcone films have lower elastic modulus than their inorganic metal oxide counterparts,[25,26] and have been found to enhance the barrier properties of ALD films.[27] In this work, we report a process for removal of hybrid metal organic thin films deposited by MLD. This initial demonstration focuses on the etching of alucone films deposited using TMA and EG. The etching mechanism we describe relies on sequential gas-phase surface reactions, but employs only organometallic precursors and does not require harsh halogen etchants.

III. Materials and Methods

Reaction Conditions:

All reactions were carried out in custom hot-walled viscous flow ALD reactors.[28] Argon carrier gas (Ar, Airgas, 99.999%) was employed at flow rates producing a background pressure of ~1.0 Torr. The conductance and pumping speed varied among the reactors used for this study, giving rise to different carrier gas flow rates among reactors between 165-270 SCCM.

1
2
3
4
5
6
7
8
9
10
11
12
13
14
15
16
17
18
19
20
21
22
23
24
25
26
27
28
29
30
31
32
33
34
35
36
37
38
39
40
41
42
43
44
45
46
47
48
49
50
51
52
53
54
55
56
57
58
59
60

Trimethylaluminum (TMA, Strem, 98%) and water (H_2O, deionized to an ionic resistance of 18.2 MΩ) precursors were held at room temperature and delivered via a virtual valve dosing scheme.[28] Ethylene glycol (EG, Sigma-Aldrich, 99.8% anhydrous) was held at 65-80°C, tertbutanol (HO^tBu, Sigma-Aldrich, 99.8% anhydrous) was held at 35-50°C, and lithium tert-butoxide (LiO^tBu, Sigma-Aldrich) and lithium hexamethyldisilizane (LiHMDS, Sigma-Aldrich, 97%) were both held at 105-120°C. EG, HO^tBu, LiO^tBu, and LiHMDS temperatures were maintained using cast aluminum jacketed heaters powered by PID temperature controllers, and delivered via a flow-over bubbler design. A partial stream of 33-45 sccm of the total inert gas flow was diverted over the headspace of each precursor for flow-over dosing. These precursors were transferred into their respective bubblers in an Ar-filled glovebox (<0.5 ppm H_2O, ~0.2 ppm O_2), and evacuated at room temperature prior to use to remove excess/dissolved gasses and impurities. Peak dosing pressures above baseline for these precursors were measured to be ~100 mTorr (EG), ~1 Torr (HO^tBu) ~10 mTorr (LiO^tBu), ~20 mTorr (LiHMDS) for the precursor temperatures specified above.

A typical dosing scheme for MLD growth of alucone consisted of 1 s TMA exposure, 10 s of Ar purge, 2 s of EG exposure, and 15 s of Ar purge. Typical dosing of HO^tBu, LiO^tBu, and LiHMDS for growth and etching experiments described below consisted of a 2-10 s precursor exposure and a 15 s Ar purge. A typical dosing scheme for MLE etching of an alucone film consisted of 5 s LiO^tBu exposure, 20 s of purge, 2 s of TMA exposure, and 15 s of purge.

Quartz Crystal Microbalance (QCM) Studies:

QCM measurements were performed at 150°C. 5 MHz gold-plated QCM crystals were loaded into an ALD QCM Sensor (Inficon). Prior to performing QCM measurements, the QCM crystal was kept in the reactor overnight to reach a steady-state temperature, and maintained within ± 0.2 °C of the setpoint using PID temperature controllers on the reactor body. Mass changes were benchmarked using ALD growth of Al_2O_3 via TMA/H_2O to confirm a mass gain per cycle (MGPC) of ~40 ng/cm^2/cycle[28,29] prior to MLD and MLE studies .

Fourier Transform Infrared (FTIR) Spectroscopy:

A smaller custom ALD reactor integrated with a Nicolet 6700 FTIR spectrometer (Thermo Scientific) was used to perform all in situ FTIR measurements. Details of the design has been reported earlier.[30] Each spectrum was collected over an average of 256 scans between 400 to 400cm^{-1} wavenumber with a 4cm^{-1} resolution. All measurements were carried out in the absorbance mode. A steel mesh loaded with ZrO_2 nanoparticles (Aldrich, < 100 nm TEM, > 25 m^2/g) was used as substrate placed between the IR beam and the liquid N_2 cooled DTGS detector to study precursor adsorption with each half ALD cycle.

Spectroscopic Ellipsometry:

Spectroscopic ellipsometry was performed using an alpha-SE instrument (J.A. Woollam) at an incident angle of 65° using a spectral range of 380-890 nm. Film properties were modeled using the CompleteEASE software package. A Cauchy model of the form $n(\lambda) = A + B/\lambda^2 + C/\lambda^3$ was employed for the the alucone films with fitted values of A = 1.493, B = 1.32×10^{-3} and C = 2.55×10^{-4}. This model fit yielded a refractive index of 1.5 at 589 nm, which is consistent with values reported previously for alucone films grown by MLD.[26]

IV. Results and Discussion

We first observed evidence of the chemical mechanism which enables MLE during QCM experiments studying the incorporation of lithium into metal organic, or metalcone films. We were attempting to improve the lithium ionic conductivity of MLD films deposited using TMA and EG (AlEG or alucone) by incorporating lithium oxide (LiO_x) using doses of LiO^tBu and H_2O[30] to form a LiO_x/AlEG laminate. Presented in Figure 1a is QCM data collected at 150°C during an attempt to deposit this LiO_x/AlEG laminate. In Figure 1a, dosing consisted of 1 s TMA dose, 10 s Ar purge, 2 s EG dose, 10 s Ar purge, 5 s LiO^tBu dose, and 10 s Ar purge. We note that in Figures 1-4, the lines at the base of each figure are location indicators for dosing and do not reflect dose pressure. For the second TMA dose (following the first dose of LiO^tBu) in Figure 1a, we observed a sharp spike in mass of 48 ng/cm^2 with an exponential decrease in mass by 18 ng/cm^2 over 10 s until the subsequent EG dose. This behavior is not observed in prior reports on alucone growth[22] or lithium aluminum oxide growth,[30] but is repeated for each TMA dose during the remainder of growth in Figure 1a. At a time of about 300 s following the start of the experiment (after the first 5 cycles of TMA/EG/LiO^tBu/H_2O) in Figure 1a, we dosed each precursor multiple times back-to-back without dosing other precursors (five times each for TMA and EG, and ten times each for LiO^tBu and H_2O) to evaluate precursor saturation behavior. During the successive pulses of EG, LiO^tBu, and H_2O, we observe typical saturation behavior expected for self-limiting growth. However, during the five successive TMA pulses, we observed a decrease in mass upon each of the five successive pulses of TMA, with an overall decrease in mass of 65.8 ng/cm^2.

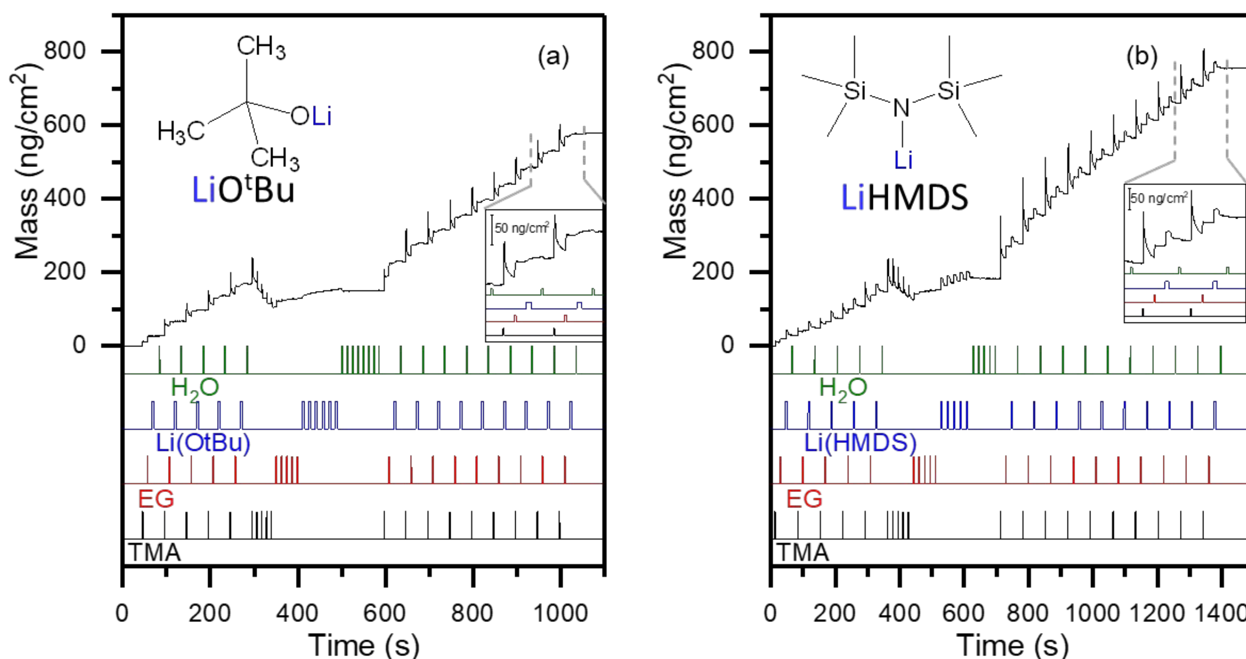

Figure 1. QCM measurements during MLD growth of (a) TMA/EG/LiO^tBu/H_2O and (b) TMA/EG/LiHMDS/H_2O including multidoses following 5 ALD cycles to measure saturation behavior. The insets show a zoomed window of the final two growth cycles.

1
2
3
4
5
6
7
8
9
10
11
12
13
14
15
16
17
18
19
20
21
22
23
24
25
26
27
28
29
30
31
32
33
34
35
36
37
38
39
40
41
42
43
44
45
46
47
48
49
50
51
52
53
54
55
56
57
58
59
60

We hypothesized initially that the mass loss we observed upon TMA exposure may have originated from residual O^tBu^- ligands in the alucone film as have been observed in prior work.[31] We suspected that upon dosing TMA, residual $OtBu^-$ ligands in the film may exchange for methyl groups from TMA, leading to a decrease in mass. In an effort to circumvent this process, we employed a second lithium organic salt (LOS) precursor, lithium hexamethyldisilizane (LiHMDS) as used in prior work,[32] and depicted in the inset in Figure 1b. In Figure 1b, dosing consisted of 1 s TMA dose, 15 s Ar purge, 2 s EG dose, 15 s Ar purge, 5 s LiHMDS dose, and 15 s Ar purge. We expected that fewer $HMDS^-$ ligands would remain in the film after LiHMDS doses because (a) $HMDS^-$ ligands are expected to form weaker bonds to surface Al* (N in $HMDS^-$ is less electronegative than the O in $OtBu^-$), and (b) the $HMDS^-$ is expected to be more sterically hindered for nucleophilic attack on surface Al* groups than $OtBu^-$. The electronegativity difference of these two ligands is reflected in the pKa values of tert-butanol (HO^tBu) and hexamethyldisilizane (HMDS), where HMDS has a lower pKa than HOtBu owing to α-silyl stabilization.[33–35] We studied the growth behavior of a LiO_x/alucone laminate using LiHMDS in Figure 1b. However, we still observed a mass decrease during five successive TMA doses at a time of 360 s in Figure 1b when using LiHMDS as the LOS precursor. The mass decrease we observe during the TMA doses when using the LiO^tBu precursor is larger (65.8 ng/cm^2) than when using the LiHMDS precursor (22.7 ng/cm^2), suggesting that the LiHMDS may have prevented some mass loss. Additionally, because the $HMDS^-$ ligand is more massive (160 g/mol) than the $OtBu^-$ ligand (74 g/mol), the smaller mass loss observed using the LiHMDS precursor corresponds to 84 % less ligand exchange on a molar basis. These data suggested that the use of $HMDS^-$ may be reducing the mass loss, or etching, effect.

These observations motivated us to try to understand to what extent this etching behavior would proceed upon TMA doses—whether it was limited to the removal of just a small fraction of the film mass, or whether etching would continue with additional TMA doses. To evaluate this, we performed 120 successive TMA doses following 15 growth cycles of TMA/EG/Li-precursor/ H_2O and measured the mass changes by QCM as presented in Figure 2. In Figure 2, dosing consisted of 0.75 s TMA doses with 10 s purge between each TMA dose. We observed that the mass on the QCM crystal continued to decrease with each successive TMA dose. We also observe that when TMA doses were stopped for short intervals (e.g. at a time of 270 s in Figure 2), the mass decrease also stopped, and resumed only when TMA doses resumed. We note that this pause was performed manually and the duration of the pause varied between the films grown using LiO^tBu and LiHMDS. Following 120 TMA doses, the etching was still proceeding at -4 ng/cm^2/TMA dose for the film grown with LiO^tBu and -1 ng/cm^2/TMA dose for the film grown with LiHMDS in Figure 2. We stopped the etching at this point and evaluated the mass loss to compare the impact of the lithium precursor on the extent of etching. The initial masses of the films deposited using 15 TMA/EG/Li-precursor/H_2O growth cycles were 578.3 ng/cm^2 using the LiO^tBu precursor and 752.5 ng/cm^2 using the LiHMDS precursor. After 120 TMA doses, we observed overall mass decreases of 441.6 ng/cm^2 and 374.8 ng/cm^2, corresponding to a loss of 76.4 % and 49.8% of the initial film thickness for films grown using the LiO^tBu precursor and LiHMDS precursor, respectively. The film grown with LiHMDS exhibited less etching than the film grown with LiO^tBu, in line with the removal of residual ligands as we hypothesized. However, the magnitude of the etching we observe for the film grown using LiO^tBu (>75 % of film mass etched) cannot be accounted for by the removal of residual ligands alone. Even if all of the EG in the alucone film were removed, this would only account for a 56% decrease in mass

1
2
3
4
5
6
7
8
9
10
11
12
13
14
15
16
17
18
19
20
21
22
23
24
25
26
27
28
29
30
31
32
33
34
35
36
37
38
39
40
41
42
43
44
45
46
47
48
49
50
51
52
53
54
55
56
57
58
59
60

corresponding to the conversion of $Al_2(OC_2H_4O)_3$ to Al_2O_3—about 20 % less mass loss than we observe using LiO^tBu.

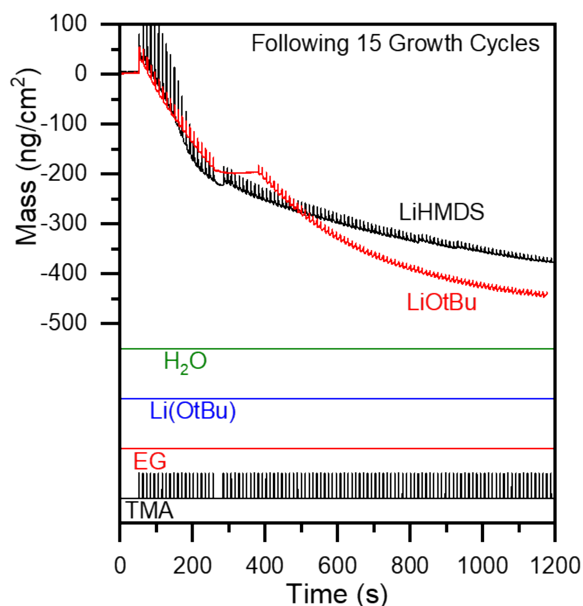

Figure 2. QCM Mass changes during TMA doses performed after 15 growth cycles of TMA/EG/Li-precursor/H_2O, where the Li-precursor used for film growth is labeled next to each trace.

Comparing our observations in Figures 1 and 2 with prior literature reports, the etching behavior we observe seems to be unique to the combination of EG, TMA, and Li precursors used here—the growth of alucone using TMA/EG and of lithium aluminum oxide using TMA/H_2O/LiO^tBu/H_2O are both well-studied,[22,30] and no etching was observed for these processes. We note that similar etching behavior was observed during the TMA in previous reports of MLD growth using TMA/hydroxyquinoline[36] and TMA/carboxylic acid,[37] but originated from reactions between the two growth precursors and was not introduced by the addition of a third precursor (here LiO^tBu). Based on the prior report studying the growth of lithium aluminum oxide, we expected that introducing more water during the growth may suppress the etching phenomenon we observed in Figure 2. In Figure 3a, we present an overlay of three QCM traces of 20 growth cycles using TMA/EG/LiHMDS/H_2O with H_2O dose times of 0 s (no dose), 2 s, and 5 s. In Figure 3a, TMA was dosed for 1 s with a 15 s Ar purge, EG was dosed for 2s with a 15 s Ar purge, and LiHMDS was dosed for 5 s with a 15 s Ar purge. We note that the total time for growth is significantly shorter with no H_2O dose owing to the removal of the H_2O purge time with no H_2O dose. We observe that for each of these samples, the final mass gain after 20 growth cycles is roughly equivalent at ~ 750 ng/cm^2 (751 ng/cm^2, 731 ng/cm^2, and 748 ng/cm^2 for the 0 s, 2 s, and 5 s water dose conditions, respectively). We note that the steady state mass gain per cycle values are different with and without the H_2O dose at 36 ng/cm^2/cycle and 43 ng/cm^2/cycle, respectively. The equivalent mass gain of ~750 ng/cm^2 after 20 cycles for each of these growth conditions is coincidental.

1
2
3
4
5
6
7
8
9
10
11
12
13
14
15
16
17
18
19
20
21
22
23
24
25
26
27
28
29
30
31
32
33
34
35
36
37
38
39
40
41
42
43
44
45
46
47
48
49
50
51
52
53
54
55
56
57
58
59
60

Following 20 TMA/EG/LiHMDS/H_2O growth cycles, we performed 40 successive TMA exposures and measured the resulting mass change as depicted in Figure 3b. In Figure 3b, each TMA dose was 0.75 s in duration with a 10 s Ar purge between each TMA dose. We observed that for the film grown using no water dose (Figure 3a), subsequent TMA exposures (Figure 3b) produced film etching of 594 ng/cm^2, or 79% of the film mass lost after 40 TMA doses, whereas when using a 5 s water dose in each growth cycle (Figure 3a), only 7 ng/cm^2 of etching, or 1% film mass loss was observed in subsequent TMA exposures (Figure 3b). Additionally, employing a 2 s water dose during growth slowed (but did not stop) the etching process to produce only 13% film mass loss after 40 subsequent TMA doses. The data in Figure 3 indicate that H_2O doses prevent the etching phenomenon perhaps because H_2O doses lead to the formation of aluminum and/or lithium oxides which are insusceptible to etching. The film etching resulting in 79% removal of the alucone films grown with interspersed LiHMDS doses further verifies that the removal of residual ligands does not account for the etching behavior we observe. We are uncertain as to why 21% of the alucone mass remained following TMA exposures, but this may arise because lithium is needed for the etching process (see below), and the lithium grown into the film in Figure 3 was depleted before the entire film was etched. We demonstrate more complete etching when additional lithium is introduced into the alucone film below.

We also note that we observe a correlation between the intensity of the mass spikes upon TMA dose in Figure 3a and the severity of etching upon TMA exposure in Figure 3b. The spikes in mass upon TMA exposure without any H_2O dose are up to >400 ng/cm^2 in height, with no such spikes observed upon TMA exposure for the film grown with a 5 s H_2O dose. While the origins of the mass spikes are unknown at this time, they may indicate absorption of the TMA precursor into the bulk alucone/LiOH film as observed during TMA/H_2O growth onto poly(methyl methacrylate) (PMMA) polymer films.[38]

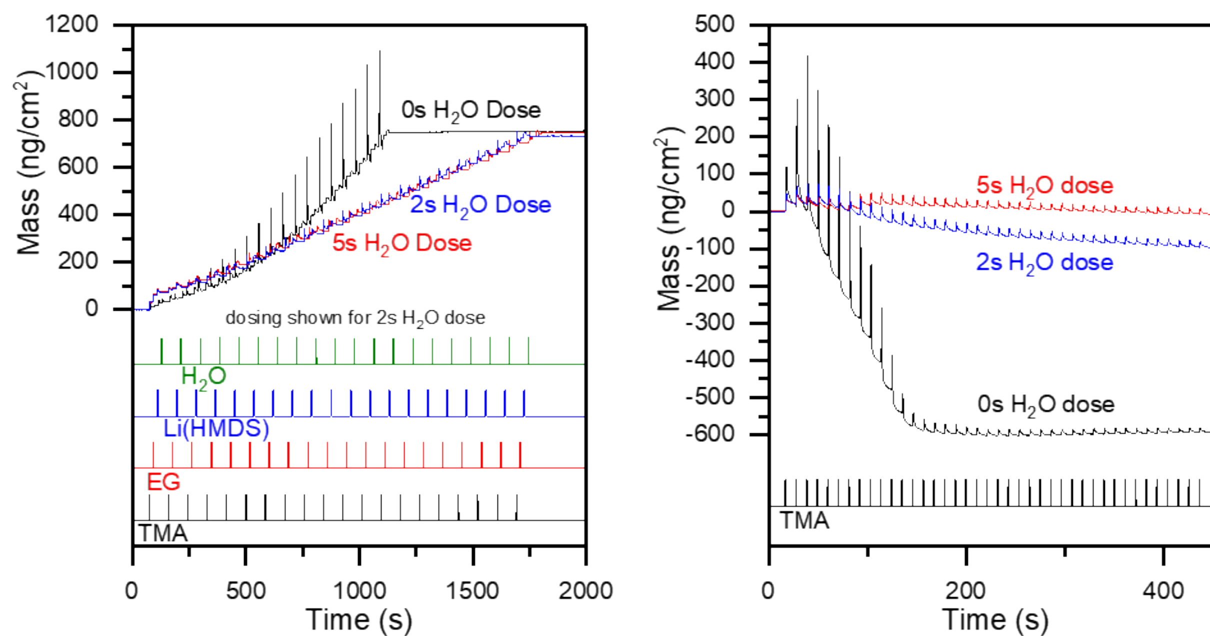

Figure 3. Impact of water dose in TMA/EG/LiHMDS/H_2O growth cycles on film etching during subsequent TMA exposures.

1
2
3
4
5
6
7
8
9
10
11
12
13
14
15
16
17
18
19
20
21
22
23
24
25
26
27
28
29
30
31
32
33
34
35
36
37
38
39
40
41
42
43
44
45
46
47
48
49
50
51
52
53
54
55
56
57
58
59
60

Based on the data in Figure 3, we concluded that introducing LOS precursors during alucone growth makes the alucone film susceptible to etching by TMA. The LOS precursor is the key difference between the experiments conducted in Figure 3 and prior reports on MLD growth using TMA/EG where no etching was observed. We expect that the LOS acts to weaken the alucone structure and allows for etching. The most straightforward explanation of this is that the LOS (e.g. LiHMDS) heterolytically cleaves Al-O bonds in R-Al-OC_2H_4O-Al-R to form, for example, R-Al-HMDS and Li-OC_2H_4O-Al-R groups. Then upon TMA exposure, -CH_3 and -Al$(CH_3)_x$ ligands act to release these groups and form volatile species. The specific mechanism for this etching behavior merits further study outside of the scope of this work, but based on this hypothesized mechanism, may include volatile compounds such as $(CH_3)_2$-Al-HMDS, CH_3-Al-$(HMDS)_2$, and Al$(HMDS)_3$; Li-OC_2H_4O-Li, Li-OC_2H_4O-Al-$(CH_3)_2$, (Li-$OC_2H_4O)_2$-Al-CH_3, and (Li-$OC_2H_4O)_3$Al; or $LiCH_3$, and CH_3-Al-$O_2C_2H_4$. The formation of larger molecular weight species by linking two Al centers is also possible, e.g. (Li-OC_2H_4O)-Al-$(OC_2H_4O)_2$-Al-(OC_2H_4O-Li). These larger molecular weight species are expected to have lower vapor pressures than the smaller molecules listed above. However, this general scheme, including larger molecular weight leaving groups, is consistent with reaction schemes observed during atomic layer etching (ALE)[7,8] and the removal of surface blocking species.[39] We also note that the $HMDS^-$ ligands written in all of the potential volatile species we list above may be replaced with $OtBu^-$ ligands to produce a series of analogous potential volatile species for etching processes using the LiO^tBu precursor.

Based on the etching observations in Figure 1-3, we were interested whether we could take advantage of the etching behavior arising from the combination of TMA and LOS precursors to etch MLD metalcone films even when no lithium was present in the film as-grown.
We expect that the same etching mechanisms we observe in Figures 1-3 above may occur at the surface of a MLD metalcone film if we introduce exposure cycles consisting of LOS precursors and TMA. In this proposed scheme, the LOS precursor (e.g. LiO^tBu) would dissociate on the surface of the MLD film. Upon TMA exposure, methyls could transfer to surface atoms which are bound to the constituents of the LOS, volatilizing them and leading to film etching. This would constitute a new form of thermal thin film etching, analogous to atomic layer etching (ALE) etching of ALD films, but for MLD films—which we term molecular layer etching, or MLE.

To evaluate whether we could achieve MLE of a metalcone film with no lithium in the film as-grown, we performed 10 growth cycles of TMA/EG to deposit alucone onto a QCM crystal and then performed 67 LiO^tBu /TMA etch cycles as depicted in Figure 4a. For growth in Figure 4, TMA was dosed for 0.75 s with a 15 s Ar purge and EG was dosed for 2 s with a 10 s Ar purge. We observe that the initial growth of TMA/EG agrees with prior literature reports with an average mass gain per cycle (MGPC) of 32 ng/cm^2/cycle at 150°C over these 10 MLD cycles.[22] When LiO^tBu and TMA are dosed, the mass begins to decrease. For etching in Figure 4a, LiO^tBu is dosed for 5 s with a 15 s purge and TMA is dosed for 1 s with a 15 s purge. After 10 LiO^tBu /TMA etching cycles, the dosing is paused for >2 minutes at a time of 829 s in Figure 4a, and we observe that the mass change does not continue to decrease until LiO^tBu and TMA doses resume. We also dosed HO^tBu/TMA plotted as a red trace in Figure 4a, and saw no etching behavior (instead observing growth) suggesting that Li is required for etching and the $OtBu^-$

1
2
3
4
5
6
7
8
9
10
11
12
13
14
15
16
17
18
19
20
21
22
23
24
25
26
27
28
29
30
31
32
33
34
35
36
37
38
39
40
41
42
43
44
45
46
47
48
49
50
51
52
53
54
55
56
57
58
59
60

ligand alone is not sufficient for etching. We note that HO^tBu/TMA cycles did not result in growth in prior work, and may arise here from the alucone underlayer versus Al_2O_3 underlayer used in this prior work.[39] We also attempted MLE using LiO^tBu and tris(dimethylamido)aluminum rather than TMA and observed no etching (not shown) and we attempted ALE of ALD Al_2O_3 using LiO^tBu and TMA and observed no etching (not shown). At a time of 1224 s in Figure 4a we replace 5 s LiO^tBu doses for 1 s TMA doses during 20 etching cycles, and observe that the rate of change in mass diminishes during this period. In Figure 4b, we plot the total cumulative mass change during the 40 TMA doses starting a time of 1224 s, and observe self-limiting behavior for the TMA exposures, where the mass change plateaus to a value of -40 ng/cm^2/cycle. The self-limiting behavior is gradual over a long exposure time and, could be characterized as soft-saturating behavior. A 20 s TMA exposure is required to reach -30 ng/cm^2/cycle and 40 s exposure is required to reach -40 ng/cm^2/cycle. When LiO^tBu is introduced again, the etch rate increases upon subsequent TMA exposure—indicating that doses of both LiO^tBu and TMA must be repeated for the etching process to continue. Using this etching method, we observe the removal of 95% of the alucone film grown using TMA/EG, with only 13 ng/cm^2 of mass remaining after etching.

1
2
3
4
5
6
7
8
9
10
11
12
13
14
15
16
17
18
19
20
21
22
23
24
25
26
27
28
29
30
31
32
33
34
35
36
37
38
39
40
41
42
43
44
45
46
47
48
49
50
51
52
53
54
55
56
57
58
59
60

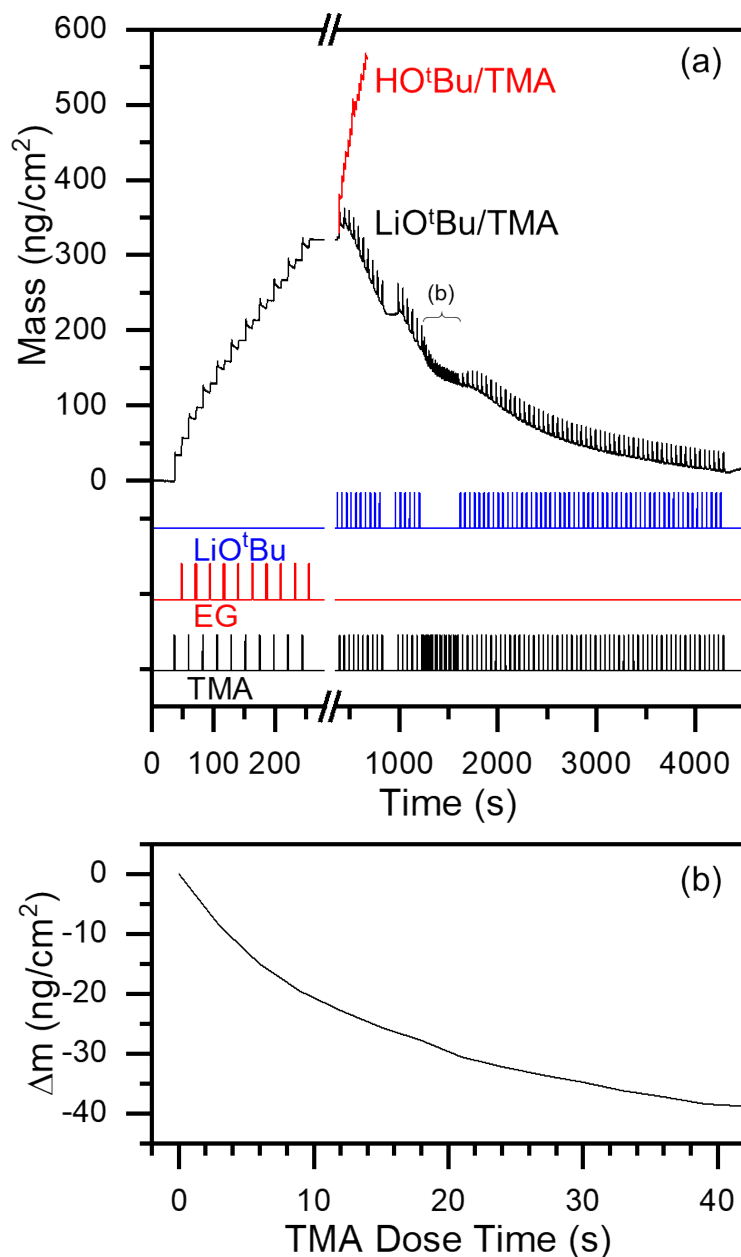

Figure 4. QCM data of (a) growth using ten cycles of TMA/EG followed by etching using 67 exposures of LiO^{t}Bu /TMA, compared with exposures of HOtBu/TMA, including (b) mass change observed during 40 successive 1 s TMA doses.

To better understand the chemical processes leading to the mass loss we observe in Figure 4, we performed Fourier transform infrared spectroscopy (FTIR) in operando during MLD of alucone using TMA and EG followed by MLE using LiO^{t}Bu and TMA. During growth, we observe an increase in absorbance with an increasing number of alucone growth cycles in Figure 5a. We observe a range of peaks in Figure 5a which are in agreement with prior studies of alucone growth.[22] These include the peak at 905 cm^{-1} from Al-O stretching vibrations, and peaks at 1086 cm^{-1} and 1132 cm^{-1} from C-O and C-C stretching vibrations, respectively. We also observe a

1
2
3
4
5
6
7
8
9
10
11
12
13
14
15
16
17
18
19
20
21
22
23
24
25
26
27
28
29
30
31
32
33
34
35
36
37
38
39
40
41
42
43
44
45
46
47
48
49
50
51
52
53
54
55
56
57
58
59
60

range of features (at 1192 cm^{-1}, 1255 cm^{-1}, and 1354-1358 cm^{-1}) associated with the CH_2 twist and CH_2 wag modes and a feature (at 1468 cm^{-1}) associated with the CH_2 scissor in the EG chain. Following 10 growth cycles of TMA/EG, we then performed 10 etch cycles using LiO^tBu and TMA. The FTIR data collected in operando during the etch cycles is presented in Figure 5b. During etching, the absorbance of all peaks decreases with increasing LiO^tBu /TMA cycles. After 10 etch cycles, some features are still present in the FTIR spectrum, indicating that the alucone film has not been entirely removed from the powder ZrO_2 substrate. The incomplete removal of 10 alucone growth cycles following 10 etch cycles is consistent with the behavior observed in Figure 4, where 100 etch cycles were required to remove 10 growth cycles of alucone film. Additionally, limited diffusion into the ZrO_2 powder may restrict the extent of etching on the FTIR samples over that observed on flat samples.

Both the data in Figure 4a and Figure 5b indicate the etching slows as the film thickness decreases. The data in Figure 4a show that the etch rate using LiO^tBu /TMA starts as high as 15 ng/cm^2/cycle during the first ten etching cycles, and then decreases to < 5 ng/cm^2/cycle during the final etch cycles. This behavior is also reflected in Figure 5b, where the absorbance of the feature at 1132 cm^{-1} decreases from 0.33 to 0.18 over the first 4 LiO^tBu /TMA cycles, but only decreases from 0.10 to 0.08 between the 6th and 10th LiO^tBu /TMA cycles. This may arise because alucone growth using EG results in double-reacted EG molecules[22] which block some growth sites, perhaps leading to a lower density film on the surface than in the bulk. A lower density alucone on the surface may allow for rapid diffusion of the TMA and Li salt precursors into the film during initial etching, but then as the film is etched, the more dense alucone is exposed which etches more slowly. This changing etch rate may also arise from a reservoir effect in the film, where species diffuse deeper into thicker films leading to a faster etching rate.

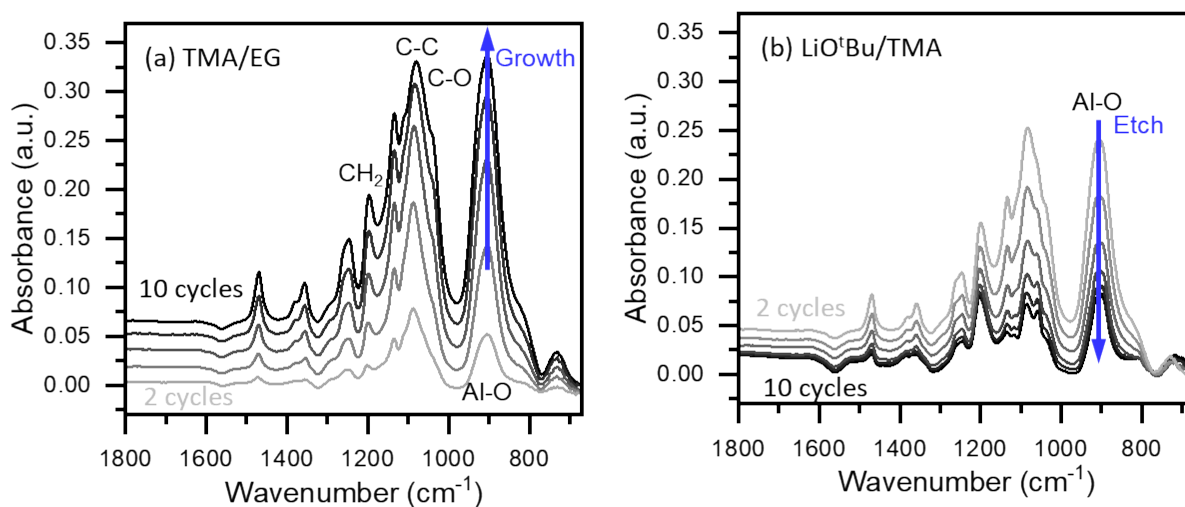

Figure 5. FTIR measurements during (a) alucone growth using 2, 4, 6, 8, and 10 cycles of MLD using TMA/EG followed by (b) 2, 4, 6, 8, and 10 cycles of MLE using LiO^tBu /TMA.

In Figure 6, we examine the FTIR difference spectra obtained during individual doses of LiO^tBu and TMA during MLE in Figure 5b. The dominant features which appear upon LiO^tBu exposures in Figure 6a and 6c exhibit symmetric, reversible, flip-flop behavior when alternating between LiO^tBu and TMA doses, as discussed below, indicating reversible chemical

1
2
3
4
5
6
7
8
9
10
11
12
13
14
15
16
17
18
19
20
21
22
23
24
25
26
27
28
29
30
31
32
33
34
35
36
37
38
39
40
41
42
43
44
45
46
47
48
49
50
51
52
53
54
55
56
57
58
59
60

transformations. Upon LiO^{t}Bu exposures (Figure 6a and 6c), we observe an increase in features at 1366 cm^{-1} and 1390 cm^{-1} which correspond to the CH_3 bending modes in $OtBu^-$, and at 2840-3000 cm^{-1} which correspond to CH_3 stretching modes in the $OtBu^-$ ligand[40] suggesting that $OtBu^-$ is present on the film surface following LiO^{t}Bu exposure. We also observe a feature at 1095 cm^{-1} in Figures 6a and 6c which corresponds to the vibrational frequency of the C-O stretching mode observed in alucone[22] and a feature at 1131 cm^{-1} which corresponds to the vibrational frequency of the C-O stretching mode observed in HOtBu molecules[40]. These two features also indicate that $OtBu^-$ ligands are present on the film surface following LiO^{t}Bu doses. We also observe features at 925 cm^{-1} and 978 cm^{-1} upon LiO^{t}Bu exposures which may be associated with rocking modes of CH_3 groups in $OtBu^-$ ligands,[40] or with Al-O stretch in alucone[22] perhaps arising from the formation of Al-O groups with O from $OtBu^-$. During subsequent TMA exposures (Figure 6b and 6d), we see the removal of all of the $OtBu^-$ features which were introduced during the LiO^{t}Bu dose except for select CH_3 stretch modes, as described further below. These data indicate that $OtBu^-$ ligands are introduced into the film during LiO^{t}Bu exposure, and are released from the film upon TMA exposure. This FTIR data is consistent with the mechanism proposed above in which LiO^{t}Bu dissociates on the surface of the alucone and heterolytically cleaves Al-O bonds in R-Al-OC_2H_4O-Al-R to form, R-Al-O^{t}Bu and Li-OC_2H_4O-Al-R surface groups.

Next we examined the FTIR data acquired upon TMA exposures following LiO^{t}Bu exposures (Figure 6b and 6d). Here, we see indication that CH_3 groups are accumulating in the film during the LiO^{t}Bu /TMA etch process. During TMA exposures, we see a distinct 0.01 increase in absorbance at 1209 cm^{-1} which corresponds to a deformation mode of CH_3 groups bound to Al, paired with an increase at 2900-2940 cm^{-1} which corresponds to the symmetric and asymmetric stretches for CH_3 bound to Al.[41] [4243] These features are in agreement with other work on TMA exposures to polymers. [38,44,45] However the increase in absorbance at 1209 cm^{-1} upon TMA dose is only partially reversed upon the next LiO^{t}Bu exposure —less than 60 % of the peak height is reflected as a decrease in absorbance at 1209 cm^{-1} upon subsequent LiO^{t}Bu exposure. Additionally, we observe an increase above the background for the CH_3 stretch region from 2900-2940 cm^{-1} during both TMA and LiO^{t}Bu exposures. The persistence of these two features suggests accumulation of CH_3 in the polymer film during etching. The accumulation of methyl groups in the film is also reflected in the overall absorption data in Figure 5. The ratio in absorbance of the CH_3 deformation feature at 1209 cm^{-1} versus the absorbance in the C-C region at 1086 cm^{-1} is ~0.5 following 10 TMA/EG growth cycles in Figure 4a, and ~1.0 following 10 subsequent LiO^{t}Bu /TMA etch cycles in Figure 4b, indicating a relative increase in CH_3 concentration versus C-C concentration in the film and supporting the conclusion that CH_3 groups are accumulating in the film. We propose that these accumulating CH_3 groups arise from the transfer of methyls to aluminum atoms in the film when TMA reacts to liberate volatile leaving groups. Accumulation of methyl groups in the surface upon TMA exposure is consistent with prior reports on ALE of Al_2O_3 using TMA and HF.[8] We also see a decrease in absorbance in the region from 800-1000 cm^{-1} following TMA exposures in Figure 6b and 6d. This region is characteristic of Al-O bonding[22] and suggests that Al-O bonds are heterolytically cleaved during the TMA dose, leading to etching. This is consistent with our QCM observations where the mass loss occurs during the TMA dose and is consistent with the mechanism proposed above in which surface Al atoms within Al-OtBu and Li-OC_2H_4O-Al-R groups are methylated upon TMA exposure to generate volatile leaving groups.

1
2
3
4
5
6
7
8
9
10
11
12
13
14
15
16
17
18
19
20
21
22
23
24
25
26
27
28
29
30
31
32
33
34
35
36
37
38
39
40
41
42
43
44
45
46
47
48
49
50
51
52
53
54
55
56
57
58
59
60

Interestingly, we also see a decrease in absorbance centered at 1563 cm^{-1} upon TMA exposures, labeled with an asterisk. This frequency region is associated with (cyclic) ethylene moities including furan,[46] benzoyl cations,[47] or n-methylvinoxide.[48] However, we do not expect these groups to be present in the alucone films, and further investigation outside the scope of this work will be required to assign the absorption loss feature at 1563 cm^{-1} observed upon TMA exposure. We also observe absorbance peaks at 1022 and 1059 cm^{-1} upon TMA exposure which are not assigned, but which flip-flop reversibly during TMA/ LiO^tBu doses.

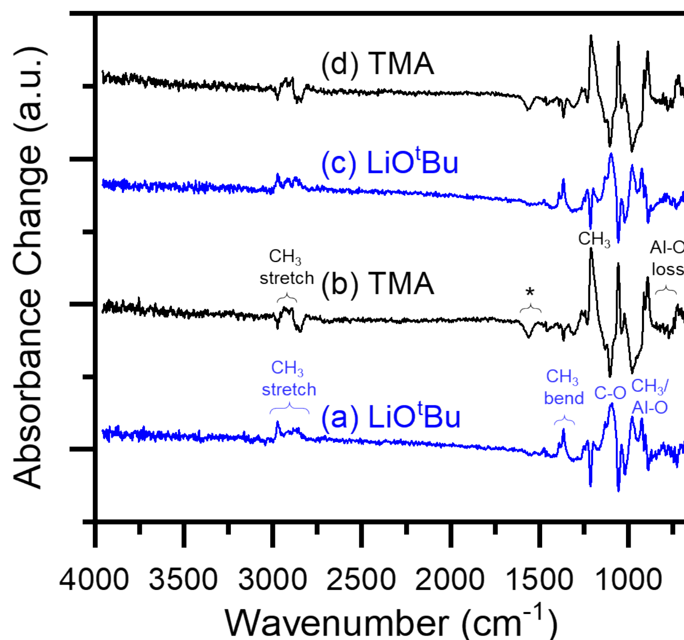

Figure 6. FTIR difference spectra for successive doses of LiO^tBu and TMA during MLE of alucone.

After establishing an understanding of the surface chemistry occurring during TMA/ LiO^tBu etching cycles in Figure 6, we explored the saturation behavior of these precursors by examining the absorbance changes with varying precursor dose times. In Figure 7, we present the cumulative absorbance change of peaks at 1131 cm^{-1} (C-O stretching in $OtBu^-$) during seven sequential 1 s LiO^tBu doses and at 1209 cm^{-1} (CH_3 deformation in Al-CH_3) during seven sequential 1 s TMA doses. These peaks were selected because they were the most prominent features observed in Figure 6 during each precursor exposure. Here, we observe that during LiO^tBu doses, the absorbance for the feature at 1131 cm^{-1} increases with increasing LiO^tBu exposure. The rate of increase in absorbance at 1131 cm^{-1} slows after about 2 s of LiO^tBu exposure, indicating some degree of self-limiting behavior. We expect that continued slow diffusion of Li^+ and $OtBu^-$ into the bulk of the alucone film with longer LiO^tBu exposure leads to the "soft" saturation behavior we observe. Conversely, during the TMA exposures, we observe that the absorbance for the prominent CH_3 deformation feature at 1209 cm^{-1} increases during the first 2 s of exposure, and then begins to decrease with a somewhat constant slope up to 7 s of exposure. We expect that this decrease in absorbance of the CH_3 deformation feature between 2-7 s of TMA exposure arises because the methylated surface of the alucone film is etching away after 2 s of TMA exposure resulting in a net loss of CH_3. In Figure 4b, we show that the TMA

1
2
3
4
5
6
7
8
9
10
11
12
13
14
15
16
17
18
19
20
21
22
23
24
25
26
27
28
29
30
31
32
33
34
35
36
37
38
39
40
41
42
43
44
45
46
47
48
49
50
51
52
53
54
55
56
57
58
59
60

exposure results in soft self-limiting behavior over 40 s of dose time based on mass changes during QCM measurements. In Figure 7, we dose TMA for only 7 s, and the curve shape does not match that observed in Figure 4b—where in Figure 4 we see a monotonic decrease in the mass during TMA exposures, but in Figure 7 we see an increase in the CH_3 absorbance with increasing TMA exposure up to 2 s exposure, followed by a decrease in CH_3 absorbance with increasing TMA exposure from 2 s to 7 s of exposure. We note that the 7 s of total TMA dose in Figure 7 is insufficient for saturation based on the data in Figure 4. The decrease in spectroscopic signal during TMA exposure in Figure 7 is expected to arise from a loss of surface species upon etching rather than saturation behavior. As such, we expect that the gravimetric data in Figure 4b are a better indicator of self-limiting behavior during TMA dose than the spectroscopic data.

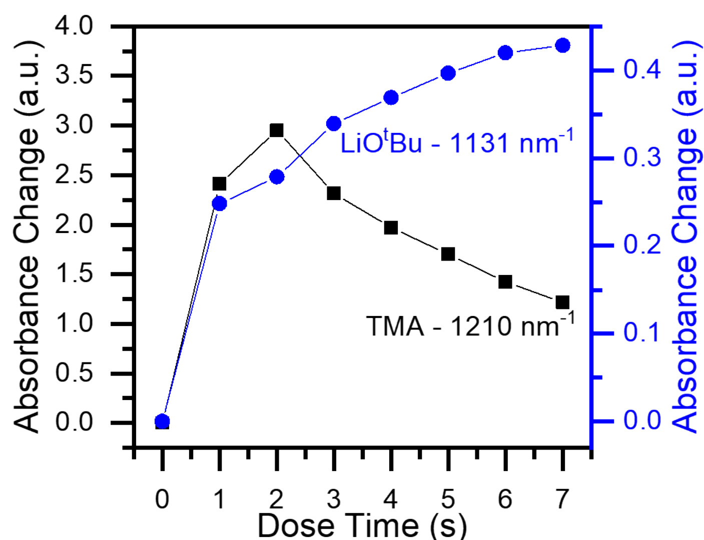

Figure 7. FTIR absorbance change versus dose time for TMA and LiO^{t}Bu doses during etching of alucone.

Based on the in-situ QCM and FTIR data presented above, we expected to be able to remove alucone films from substrates with nm-scale resolution using LiO^{t}Bu /TMA etching. We demonstrate ex-situ etching of alucone from silicon wafers in Figure 8. For these experiments, 200 TMA/EG growth cycles were used to deposit alucone on a series of ~1” x ~1” silicon wafers, resulting in a total average thickness of 377 +/- 8 Å for all samples. These alucone-coated silicon wafers were transferred to an argon-filled glovebox (<1 ppm H_2O) connected directly to the ALD reactor used for alucone growth. The samples were stored in the argon-filled glovebox to limit water exposure. Water exposure is expected to prevent MLE as depicted in Figure 3. Three samples at a time were placed back into the ALD reactor attached to the glovebox and varying numbers of LiO^{t}Bu /TMA etching cycles were performed at one of three different temperatures: 160°C, 200°C and 266°C, as depicted in Figure 8a. Following etching, the silicon wafers were removed from the reactor, then transferred out of the argon-filled glovebox. Final film thicknesses were characterized using spectroscopic ellipsometry promptly after transferring each sample out of the glovebox environment. The thickness values in Figure 8a represent average values for the three samples in each experiment, and the error bars represent the standard deviations of these measurements.

1
2
3
4
5
6
7
8
9
10
11
12
13
14
15
16
17
18
19
20
21
22
23
24
25
26
27
28
29
30
31
32
33
34
35
36
37
38
39
40
41
42
43
44
45
46
47
48
49
50
51
52
53
54
55
56
57
58
59
60

At each temperature we observed a decrease in film thickness with increasing LiO^{t}Bu /TMA cycles where the etch rate increased with increasing temperature. At 160 °C the etch rate corresponds to -4 Å/cycle, at 200 °C the etch rate corresponds to -10 Å/cycle, and at 266 °C the etch rate corresponds to -36 Å/cycle. Assuming an alucone density of 1.5 g/cm^3,[22] these etch rates corresponds to -60 ng/cm^2/cycle, -150 ng/cm^2/cycle, and -540 ng/cm^2/cycle for 160°C, 200°C and 266°C, respectively. These etch rates are higher than the etch rate of 15 ng/cm^2/cycle observed at 150°C in Figure 4 above. This lower etch rate for the QCM studies is related to differences in the delivery of the LiO^{t}Bu precursor between the two experiments. The LiO^{t}Bu was undersaturated (10 mTorr peak partial pressure) during the initial QCM experiments in Figure 4, and improvements in the LiO^{t}Bu precursor delivery provided saturating LiO^{t}Bu doses (10 mTorr sustained partial pressure) in Figures 5-8. Based on the etch rates observed in Figure 8a, we performed an Arrhenius analysis to arrive at a thermal activation barrier for the etching process in Figure 8b following procedures reported previously.[6,16] This analysis assumes Langmuir adsorption behavior of the etchant precursors with a first order Taylor series expansion approximation of the Langmuir expression for time-dependant fractional surface coverage, as outlined in the Supporting Information. This analysis resulted in a predicted activation barrier of 0.44 eV (10 kcal/mol). We suspect that diffusion of Li^+ and $OtBu^-$ and/or TMA into the bulk of the film limits the extent of etching, and drives the increased etch rate at higher temperatures. The bond strength of TMA complexation with PMMA was calculated to be -0.477 eV in a prior report, which is consistent with the energy we observe and suggests TMA hopping is the barrier to etching.[49]

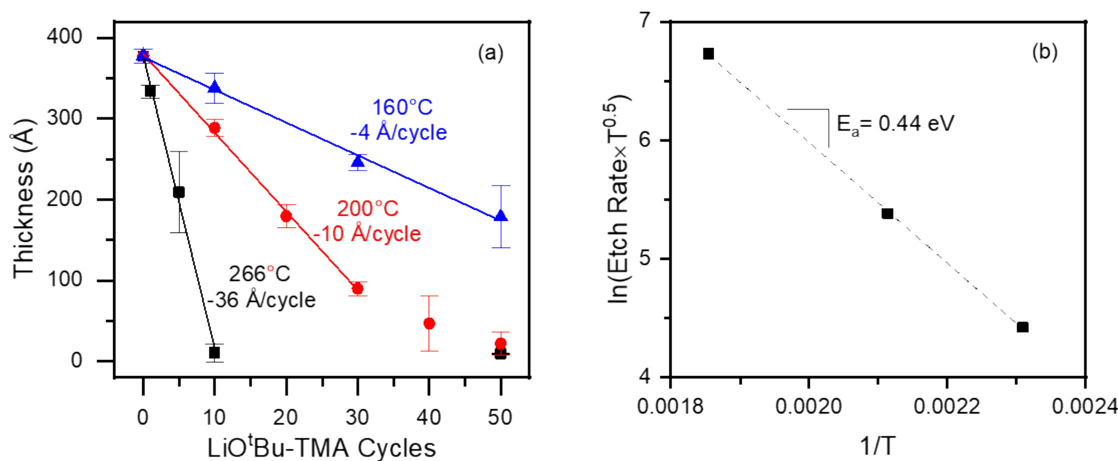

Figure 8. Study of temperature dependence on etch rate of alucone using LiO^{t}Bu /TMA including (a) thickness of alucone films with initial thickness of 377 nm following LiO^{t}Bu /TMA exposures between 160°C and 266°C as measured using spectroscopic ellipsometry on silicon wafers and (b) Arrhenius analysis of etch rate.

The temperature dependence of the MLE mechanism we report is qualitatively consistent with previous results for thermal ALE. For example, thermal ALE of Al_2O_3 using tin(II) acetylacetonate ($Sn(acac)_2$) and HF produced etch rates ranging from 0.14 Å/cycle at 150°C to 0.61Å/cycle at 250°C with an activation barrier of 6.6 kcal/mol.[6] Similarly, thermal ALE of WO_3 using BCl_3 and HF produced etch rates ranging from 0.55 Å/cycle at 128°C to 4.19 Å/cycle at 207°C with an activation barrier of 8.6 kcal/mol.[16] However, we observe much higher etch rates

1
2
3
4
5
6
7
8
9
10
11
12
13
14
15
16
17
18
19
20
21
22
23
24
25
26
27
28
29
30
31
32
33
34
35
36
37
38
39
40
41
42
43
44
45
46
47
48
49
50
51
52
53
54
55
56
57
58
59
60

for MLE, ranging from 4 Å/cycle at 166°C to 36 Å/cycle at 266°C with an activation barrier of 11 kcal/mol. The larger values of etch rates we observe for MLE are expected to arise from the removal of molecular units in MLE as compared with the removal of atomic species in ALE. These more rapid etch rates provided by MLE allow for faster processing for removal of MLD films.

V. Conclusions

In this work, we report the discovery of a gas phase thermal chemical process which enables the removal of metal organic thin films deposited by MLD, which we term molecular layer etching, or MLE. The MLE process takes place in MLD films upon chemical exposures of TMA and a LOS (LiO^tBu or LiHMDS). We demonstrate both (a) the rapid removal of bulk alucone films predoped with a LOS using TMA exposures and (b) the precise layer-by-layer removal of alucone films using sequential exposures of TMA and a LOS exhibiting self-limiting behavior. In operando FTIR and QCM experiments suggest that the etching mechanism initiates by LOS (e.g. LiO^tBu) heterolytically cleaving Al-O bonds in the R-Al-OC_2H_4O-Al-R alucone structure to form R-Al-OtBu and Li-OC_2H_4O-Al-R groups. Then, upon TMA exposure, the Al atoms in these alucone groups are methylated to generate volatile species. MLE is verified on silicon wafers and produce etch rates ranging from 0.4 nm/cycle at 160°C up to 3.6 nm/cycle at 266°C. We also observe the ability to prevent the etching behavior by introducing water pulses during the MLD growth, suggesting that the etching mechanism is selective to the MLD films and is not active on ALD oxides.

The ability to etch MLD metalcone films we demonstrate in this work may prove to allow metalcones to be used as nanoscale sacrificial resist layers in conventional semiconductor device manufacturing, for organic semiconductor applications, or for micro- and nano-scale electromechanical machines (MEMS and NEMS). In contrast to ALE etching processes which largely require the use HF, the MLE process we report is halogen-free and uses only organometallic vapors. In addition to the added safety afforded by avoiding HF, the low elastic modulus of metalcone films relative to metal oxides[26] may also allow MLD films to be applied as sacrificial layers for flexible electronics device manufacturing. Furthermore, the ability to selectively etch MLD layers without impacting ALD layers will allow a pathway for fabrication of small mechanical feature sizes during semiconductor device manufacturing by selectively etching the MLD films using MLE. This could be used as for precise etching of low-dielectric constant (low-k) interlayer dielectrics, for precise removal of lithography mask layers, or to synthesize novel organic or hybrid nanomaterials. We note that the use of alkali elements (e.g. Li here) prevents implementation into current semiconductor manufacturing fabrication lines because of the undesired effect on electronic properties of silicon. Nonetheless, the MLE mechanism we report may be amenable with next generation fabrication processes, or drive the discovery of alternative MLE etching mechanisms which do not require alkali elements.

The temperature dependence of the etching mechanism we observe opens up new potential avenues for control of the microstructure of MLD films. For example, one could envision exploiting this temperature-dependent etch rate to pattern alucone using laser heating. This could provide new fabrication techniques for nanoscale 3D architectures, or could be used in combination with additive manufacturing to generate high resolution feature sizes. In general, the pathway for removal of MLD films provides a new tool for the fabrication of novel nanoscale

1
2
3 geometries, and is expected to enable new frontiers in the fabrication of nano-engineered
4 materials, especially soft materials.
5
6
7 ## VI. Acknowledgements
8
9 This research was supported as part of the Center for Electrochemical Energy Science, an Energy
10 Frontier Research Center funded by the U.S. Department of Energy, Office of Science, Office of
11 Basic Energy Sciences. Use of the Center for Nanoscale Materials was supported by the U.S.
12 Department of Energy, Office of Science, Office of Basic Energy Sciences, under Contract DE-
13 AC02-06CH11357. M.J.Y. acknowledges partial support from faculty start-up funds provided by
14 the University of Missouri.
15
16
17 ## VII. Supporting Information
18 The Supporting Information contains a discussion of activation energy analysis for the etching
19 mechanism described in the text. A derivation and analysis of the activation energy using an
20 exponential expression for Langmuir adsorption is performed and compared against the first
21 order Taylor series expansion we employ for evaluating the activation energy.
22
23
24 ## VIII. References
25 (1) More, G. E. Cramming More Components Onto Integrated Circuits. *Electronics* **1965**, *38*
26 (8), 1–4.
27
28 (2) Limited, T. S. M. C. 7nm Technology
29 https://www.tsmc.com/english/dedicatedFoundry/technology/7nm.htm (accessed Jul 6,
30 2019).
31 (3) Hisamoto, D.; Kaga, T.; Takeda, E. Impact of the Vertical SOI "DELTA" Structure on
32 Planar Device Technology. *IEEE Trans. Electron Devices* **1991**, *38* (6), 1419–1424.
33 https://doi.org/10.1109/16.81634.
34 (4) Singh, N.; Agarwal, A.; Bera, L. K.; Liow, T. Y.; Yang, R.; Rustagi, S. C.; Tung, C. H.;
35 Kumar, R.; Lo, G. Q.; Balasubramanian, N.; et al. High-Performance Fully Depleted
36 Silicon Nanowire (Diameter ≤ 5 Nm) Gate-All-around CMOS Devices. *IEEE Electron*
37 *Device Lett.* **2006**, *27* (5), 383–386. https://doi.org/10.1109/LED.2006.873381.
38
39 (5) George, S. M. Atomic Layer Deposition: An Overview. *Chem. Rev.* **2010**, *110* (1), 111–
40 131. https://doi.org/10.1021/cr900056b.
41 (6) Lee, Y.; Dumont, J. W.; George, S. M. Mechanism of Thermal Al_2O_3 Atomic Layer
42 Etching Using Sequential Reactions with $Sn(Acac)_2$ and HF. *Chem. Mater.* **2015**, *27* (10),
43 3648–3657. https://doi.org/10.1021/acs.chemmater.5b00300.
44
45 (7) Lee, Y.; Dumont, J. W.; George, S. M. Atomic Layer Etching of Al_2O_3 Using Sequential,
46 Self-Limiting Thermal Reactions with $Sn(Acac)_2$ and Hydrogen Fluoride. *J. Phys. Chem.*
47 *C* **2015**, *119* (45), 25385–25393. https://doi.org/10.1021/acs.jpcc.5b07236.
48 (8) Lee, Y.; Dumont, J. W.; George, S. M. Trimethylaluminum as the Metal Precursor for the
49 Atomic Layer Etching of Al_2O_3 Using Sequential, Self-Limiting Thermal Reactions.
50 *Chem. Mater.* **2016**, *28* (9), 2994–3003. https://doi.org/10.1021/acs.chemmater.6b00111.
51
52 (9) Lee, Y.; Dumont, J. W.; Cavanagh, A. S.; George, S. M. Atomic Layer Deposition of AlF_3
53 Using Trimethylaluminum and Hydrogen Fluoride. *J. Phys. Chem. C* **2015**, *119* (25),
54 14185–14194. https://doi.org/10.1021/acs.jpcc.5b02625.
55 (10) Abdulagatov, A. I.; George, S. M. Thermal Atomic Layer Etching of Silicon Using O_2,
56
57
58
59
60

HF, and $Al(CH_3)_3$ as the Reactants. *Chem. Mater.* **2018**, *30* (23), 8465–8475. https://doi.org/10.1021/acs.chemmater.8b02745.
(11) DuMont, J. W.; Marquardt, A. E.; Cano, A. M.; George, S. M. Thermal Atomic Layer Etching of SiO_2 by a "Conversion-Etch" Mechanism Using Sequential Reactions of Trimethylaluminum and Hydrogen Fluoride. *ACS Appl. Mater. Interfaces* **2017**, *9* (11), 10296–10307. https://doi.org/10.1021/acsami.7b01259.
(12) Lee, Y.; DuMont, J. W.; George, S. M. Atomic Layer Etching of HfO_2 Using Sequential, Self-Limiting Thermal Reactions with $Sn(Acac)_2$ and HF. *ECS J. Solid State Sci. Technol.* **2015**, *4* (6), N5013–N5022. https://doi.org/10.1149/2.0041506jss.
(13) Zywotko, D. R.; George, S. M. Thermal Atomic Layer Etching of ZnO by a "Conversion-Etch" Mechanism Using Sequential Exposures of Hydrogen Fluoride and Trimethylaluminum. *Chem. Mater.* **2017**, *29* (3), 1183–1191. https://doi.org/10.1021/acs.chemmater.6b04529.
(14) Lemaire, P. C.; Parsons, G. N. Thermal Selective Vapor Etching of TiO_2: Chemical Vapor Etching via WF_6 and Self-Limiting Atomic Layer Etching Using WF_6 and BCl_3. *Chem. Mater.* **2017**, *29* (16), 6653–6665. https://doi.org/10.1021/acs.chemmater.7b00985.
(15) Lee, Y.; George, S. M. Thermal Atomic Layer Etching of Titanium Nitride Using Sequential, Self-Limiting Reactions: Oxidation to TiO_2 and Fluorination to Volatile TiF_4. *Chem. Mater.* **2017**, *29* (19), 8202–8210. https://doi.org/10.1021/acs.chemmater.7b02286.
(16) Johnson, N. R.; George, S. M. WO_3 and W Thermal Atomic Layer Etching Using "Conversion-Fluorination" and "Oxidation-Conversion-Fluorination" Mechanisms. *ACS Appl. Mater. Interfaces* **2017**, *9* (39), 34435–34447. https://doi.org/10.1021/acsami.7b09161.
(17) George, S. M.; Lee, Y. Prospects for Thermal Atomic Layer Etching Using Sequential, Self-Limiting Fluorination and Ligand-Exchange Reactions. *ACS Nano* **2016**, *10* (5), 4889–4894. https://doi.org/10.1021/acsnano.6b02991.
(18) Lee, Y.; Huffman, C.; George, S. M. Selectivity in Thermal Atomic Layer Etching Using Sequential, Self-Limiting Fluorination and Ligand-Exchange Reactions. *Chem. Mater.* **2016**, *28* (21), 7657–7665. https://doi.org/10.1021/acs.chemmater.6b02543.
(19) Kubono, A.; Okui, N. Polymer Thin Films Prepared by Vapor Deposition. *Prog. Polym. Sci.* **1994**, *19* (3), 389–438. https://doi.org/10.1016/0079-6700(94)90001-9.
(20) George, S. M.; Yoon, B.; Dameron, A. A. Surface Chemistry for Molecular Layer Deposition of Organic and Hybrid Organic−Inorganic Polymers. *Acc. Chem. Res.* **2009**, *42* (4), 498–508. https://doi.org/10.1021/ar800105q.
(21) Yoshimura, T.; Tatsuura, S.; Sotoyama, W. Polymer Films Formed with Monolayer Growth Steps by Molecular Layer Deposition. *Appl. Phys. Lett.* **1991**, *59* (4), 482–484. https://doi.org/10.1063/1.105415.
(22) Dameron, A. A.; Seghete, D.; Burton, B. B.; Davidson, S. D.; Cavanagh, A. S.; Bertrand, J. A.; George, S. M. Molecular Layer Deposition of Alucone Polymer Films Using Trimethylaluminum and Ethylene Glycol. *Chem. Mater.* **2008**, *20* (10), 3315–3326. https://doi.org/10.1021/cm7032977.
(23) Nilsen, O.; Klepper, K.; Nielsen, H.; Fjellvåg, H. Deposition of Organic- Inorganic Hybrid Materials by Atomic Layer Deposition. In *ECS Transactions*; ECS, 2008; Vol. 16, pp 3–14. https://doi.org/10.1149/1.2979975.
(24) Yoon, B.; O'Patchen, J. L.; Seghete, D.; Cavanagh, A. S.; George, S. M. Molecular Layer Deposition of Hybrid Organic-Inorganic Polymer Films Using Diethylzinc and Ethylene

1
2
3
4
5
6
7
8
9
10
11
12
13
14
15
16
17
18
19
20
21
22
23
24
25
26
27
28
29
30
31
32
33
34
35
36
37
38
39
40
41
42
43
44
45
46
47
48
49
50
51
52
53
54
55
56
57
58
59
60

Glycol. *Chem. Vap. Depos.* **2009**, *15* (4–6), 112–121. https://doi.org/10.1002/cvde.200806756.
(25) Lee, B. H.; Yoon, B.; Abdulagatov, A. I.; Hall, R. A.; George, S. M. Growth and Properties of Hybrid Organic-Inorganic Metalcone Films Using Molecular Layer Deposition Techniques. *Adv. Funct. Mater.* **2013**, *23* (5), 532–546. https://doi.org/10.1002/adfm.201200370.
(26) Lee, B. H.; Yoon, B.; Anderson, V. R.; George, S. M. Alucone Alloys with Tunable Properties Using Alucone Molecular Layer Deposition and Al_2O_3 Atomic Layer Deposition. *J. Phys. Chem. C* **2012**, *116* (5), 3250–3257. https://doi.org/10.1021/jp209003h.
(27) Park, M.; Oh, S.; Kim, H.; Jung, D.; Choi, D.; Park, J. S. Gas Diffusion Barrier Characteristics of Al_2O_3/Alucone Films Formed Using Trimethylaluminum, Water and Ethylene Glycol for Organic Light Emitting Diode Encapsulation. *Thin Solid Films* **2013**, *546*, 153–156. https://doi.org/10.1016/j.tsf.2013.05.017.
(28) Elam, J. W.; Groner, M. D.; George, S. M. Viscous Flow Reactor with Quartz Crystal Microbalance for Thin Film Growth by Atomic Layer Deposition. *Rev. Sci. Instrum.* **2002**, *73* (8), 2981. https://doi.org/10.1063/1.1490410.
(29) Wind, R. A.; George, S. M. Quartz Crystal Microbalance Studies of Al_2O_3 Atomic Layer Deposition Using Trimethylaluminum and Water at 125 C. *J. Phys. Chem. A* **2010**, *114*, 1281–1289. https://doi.org/10.1021/jp9049268.
(30) Comstock, D. J.; Elam, J. W. Mechanistic Study of Lithium Aluminum Oxide Atomic Layer Deposition. *J. Phys. Chem. C* **2013**, *117* (4), 1677–1683. https://doi.org/10.1021/jp308828p.
(31) Meng, X.; Comstock, D. J.; Fister, T. T.; Elam, J. W. Vapor-Phase Atomic-Controllable Growth of Amorphous Li_2S for High-Performance Lithium-Sulfur Batteries. *ACS Nano* **2014**, *8* (10), 10963–10972. https://doi.org/10.1021/nn505480w.
(32) Lee, Y.; Sun, H.; Young, M. J.; George, S. M. Atomic Layer Deposition of Metal Fluorides Using HF-Pyridine as the Fluorine Precursor. *Chem. Mater.* **2016**, *28* (7), 2022–2032. https://doi.org/10.1021/acs.chemmater.5b04360.
(33) Fraser, R. R.; Mansour, T. S.; Savard, S. Acidity Measurements on Pyridines in Tetrahydrofuran Using Lithiated Silylamines. *J. Org. Chem.* **1985**, *50* (17), 3232–3234. https://doi.org/10.1021/jo00217a050.
(34) Wetzel, D. M.; Brauman, J. I. Quantitative Measure of α-Silyl Carbanion Stabilization. The Electron Affinity of (Trimethylsilyl)Methyl Radical. *J. Am. Chem. Soc.* **1988**, *110* (25), 8333–8336. https://doi.org/10.1021/ja00233a008.
(35) Tabassum, S.; Sereda, O.; Reddy, P. V. G.; Wilhelm, R. Hindered Brønsted Bases as Lewis Base Catalysts. *Org. Biomol. Chem.* **2009**, *7* (19), 4009–4016. https://doi.org/10.1039/b908899g.
(36) Nilsen, O.; Haug, K. R.; Finstad, T. Molecular Hybrid Structures by Atomic Layer Deposition - Deposition of Alq_3, Znq_2 and Tiq_4 (q = 8-Hydroxyquinoline). *Chem. Vap. Depos.* **2013**, *19* (4–6), 174–179. https://doi.org/10.1002/cvde.201207043.
(37) Klepper, K. B.; Nilsen, O.; Hansen, P.-A.; Fjellvåg, H. Atomic Layer Deposition of Organic–Inorganic Hybrid Materials Based on Saturated Linear Carboxylic Acids. *Dalt. Trans.* **2011**, *40* (17), 4636. https://doi.org/10.1039/c0dt01716g.
(38) Wilson, C. A.; Grubbs, R. K.; George, S. M. Nucleation and Growth during Al_2O_3 Atomic Layer Deposition on Polymers. *Chem. Mater.* **2005**, *17* (23), 5625–5634.

https://doi.org/10.1021/cm050704d.
(39) Yanguas-Gil, A.; Libera, J. A.; Elam, J. W. Modulation of the Growth per Cycle in Atomic Layer Deposition Using Reversible Surface Functionalization. *Chem. Mater.* **2013**, *25* (24), 4849–4860. https://doi.org/10.1021/cm4029098.
(40) Korppi-Tommola, J. Tert-Butyl Alcohol-Matrix i.r. Spectra and Vibrational Assignment. *Spectrochim. Acta Part A Mol. Spectrosc.* **1978**, *34* (11), 1077–1085. https://doi.org/10.1016/0584-8539(78)80130-5.
(41) O'Brien, R. J.; Ozin, G. A. A Gas-Phase Raman Study of Trimethylaluminium and Trimethylboron Monomers. *J. Chem. Soc. A Inorganic, Phys. Theor. Chem.* **1971**, No. 1136, 1136–1138. https://doi.org/10.1039/J19710001136.
(42) Kvisle, S.; Rytter, E. Infrared Matrix Isolation Spectroscopy of Trimethylgallium, Trimethylaluminium and Triethylaluminium. *Spectrochim. Acta Part A Mol. Spectrosc.* **1984**, *40* (10), 939–951. https://doi.org/10.1016/0584-8539(84)80153-1.
(43) Atiya, G. A.; Grady, A. S.; Russell, D. K.; Claxton, T. A. Vibrational Spectra of Monomeric Trimethylaluminium and Trimethylgallium. *Spectrochim. Acta Part A Mol. Spectrosc.* **1991**, *47* (3–4), 467–476. https://doi.org/10.1016/0584-8539(91)80124-2.
(44) Gong, B.; Parsons, G. N. Quantitative in Situ Infrared Analysis of Reactions between Trimethylaluminum and Polymers during Al_2O_3 Atomic Layer Deposition. *J. Mater. Chem.* **2012**, *22* (31), 15672–15682. https://doi.org/10.1039/c2jm32343e.
(45) Biswas, M.; Libera, J. A.; Darling, S. B.; Elam, J. W. New Insight into the Mechanism of Sequential Infiltration Synthesis from Infrared Spectroscopy. *Chem. Mater.* **2014**, *26* (21), 6135–6141. https://doi.org/10.1021/cm502427q.
(46) Shimanouchi, T. *Tables of Molecular Vibrational Frequencies Consolidated Volume I*; National Bureau of Standards: Washington, D.C., 1972.
(47) Baggott, J. E.; Clase, H. J.; Mills, I. M. CH Local Modes in Cyclobutene-I. FTIR Studies 700-9000 Cm^{-1}. *Spectrochim. Acta Part A Mol. Spectrosc.* **1986**, *42* (2–3), 319–334. https://doi.org/10.1016/0584-8539(86)80195-7.
(48) Yacovitch, T. I.; Garand, E.; Neumark, D. M. Slow Photoelectron Velocity-Map Imaging of the i-Methylvinoxide Anion. *J. Phys. Chem. A* **2010**, *114* (42), 11091–11099. https://doi.org/10.1021/jp101930b.
(49) Waldman, R. Z.; Jeon, N.; Mandia, D. J.; Heinonen, O.; Darling, S. B.; Martinson, A. B. F. Sequential Infiltration Synthesis of Electronic Materials: Group 13 Oxides via Metal Alkyl Precursors. *Chem. Mater.* **2019**, *31* (14), 5274–5285. https://doi.org/10.1021/acs.chemmater.9b01714.

1
2
3
4
5
6
7
8
9
10
11
12
13
14
15
16
17
18
19
20
21
22
23
24
25
26
27
28
29
30
31
32
33
34
35
36
37
38
39
40
41
42
43
44
45
46
47
48
49
50
51
52
53
54
55
56
57
58
59
60